Effect of Aliphatic Chain Length on Polyamide

Strain Response

Quanpeng Yang,[†] Wenjun Li,[‡] Spencer T. Stober,[‡] Adam B. Burns,[‡] Manesh Gopinadhan,[‡] and Ashlie Martini*,[†]

†Department of Mechanical Engineering, University of California-Merced, 5200 N. Lake
Road, Merced, California 95343, United States

‡ExxonMobil Research and Engineering Company, 1545 Route 22 East, Annandale, New Jersey 08801, United States

E-mail: amartini@ucmerced.edu

Abstract

Reactive molecular dynamics simulations were used to model poly(p-phenylene) terephthalamide) and related aromatic-aliphatic polyamides derived from aliphatic diacids with different numbers of carbon atoms in the aliphatic chain. Tensile strain was applied to each polymer crystal in the chain direction and the mechanical response was characterized. The elastic modulus at high strain was similar for all polymers, but the modulus calculated at low strain decreased with increasing aliphatic chain length. The decrease in modulus with chain length was explained by the observation that polymers with longer aliphatic chains were wavier at equilibrium conditions such that they could accommodate low strain without stretching covalent bonds. Extension of wavy chains occurred through an intra-chain process for all polymers, quantified by the bond dihedral angles. In addition, for polymers with an even number of non-aromatic carbons, the strain response involved inter-chain slip. The ultimate stress of the polymers

exhibited an odd-even effect which was explained by ring-ring coplanarity where polymers with an even number of carbon atoms had less ring alignment and therefore lower ultimate stress. The results revealed direct correlations between aliphatic chain length, inter- and intra-chain interactions, and the mechanical properties of polyamides.

Introduction

Aromatic polyamides (i.e., aramids), the most common of which is poly(p-phenylene terephthalamide) (PPTA), are well-known for their excellent mechanical properties (superior strengthto-weight ratio and flexibility), ^{1,2} thermal stability (thermal decomposition temperature of 500° C), ^{3,4} and chemical resistance (to acid, alkali and organic solvent). ⁵⁻⁹ These properties make PPTA ideal for many different uses, including aerospace and military applications (e.g., bulletproof body armor fabric and ballistic composites) where performance-to-weight ratio is critical. ^{10–13}

However, there are limitation of PPTA, primarily associated with processability due to its high melting temperature ($\sim 500^{\circ}$ C) and poor solubility (only soluble in highly aggressive polar solvents, such as concentrated sulfuric acid). These make the processing of PPTA challenging, expensive, and environmentally unfriendly, and directly limit its wider application. ^{14–19}

Over the past decade, extensive research has been conducted to develop materials with properties comparable to PPTA but with potentially better processability. The high melting temperature of PPTA is a result of its rigid and extended conformation, which is due to the rigidity of the aramid backbone and strong intermolecular interactions such as hydrogen bonding (H-bonding) and π -stacking. ^{11,20–23} A variety of methods have been attempted using chemical modification to lower the melting temperature, including introducing bulky, packing-disruptive groups into the polymer chain or as side-groups, incorporating flexible groups into the polymer backbone, and using meta-oriented or asymmetrically substituted monomers. ^{24–31} One such approach is to combine the rigidity of aromatic moieties and the

flexibility of aliphatic moieties to create so-called aromatic-aliphatic polyamides. 11,32–36

It is expected that even minor changes in the molecular structure of the aromatic-aliphatic polyamides might significantly affect mechanical behavior. However, experimentally studying this relationship is challenging because measuring micrometer length scale polyamide crystals is difficult and time-consuming, and requires sensitive equipment. 5,37,38 In addition, it is difficult to distinguish the relative contributions of intramolecular (e.g., covalent bonds) interactions and intermolecular interactions (e.g., H-bonding and π -stacking). 39

To overcome these limitations, experimental methods have been complemented by molecular dynamics (MD) simulations to study materials at the atomistic scale. MD simulations can help interpret experimental results, guide the development of new experimental methods, and provide useful information about both the dynamic and static properties of molecular systems. MD simulations have been successfully applied to study aromatic-aliphatic polyamide crystals, including the role of aliphatic and aromatic groups on intermolecular interactions, free volume, and glass transition temperature, 31,43 the origin of melting, 11 and the influence of methylene segments on crystal packing and chain conformation. 11

However, MD simulation-based studies of the relationship between crystal structure and mechanical properties of polyamides have not been performed. Particularly, simulations have not been used to understand the effect of the length of flexible aliphatic moieties on mechanical properties. In our previous study, ⁴⁴ we compared PPTA with one PPTA-related aromatic-aliphatic polyamide, PAP5, where 5 refers to the number of carbon atoms in the diacid monomer that used in the reaction with *p*-phenylene diamine. The results showed that the mechanical properties (tensile strength and failure strain) of PAP5 were superior to those of PPTA.

Here, we extended our previous study by modeling PPTA and a homologous set of PPTA-related aromatic-aliphatic polyamides, PAP5, PAP6, PAP7, and PAP8, with 5, 6, 7 or 8 carbon atoms in the diacid monomer. The goal was to characterize the effect of aliphatic chain length on mechanical properties and then correlate differences between properties to

intra- and inter-molecular interactions and behavior.

Methods

The polymer crystal models were initially constructed using Materials Studio. ⁴⁵ For PPTA and PAP5, the unit cell lattice parameters were set to match those measured from X-ray diffraction. ¹¹ PAP6 - PAP8 were modeled based on the lattice parameters of PAP5 by simply extending the aliphatic chain length correspondingly. The chemical formulas and atomic-scale models of PPTA and PAP5 - PAP8 unit cells are shown in Fig. 1. The chain direction was aligned with the x-axis, and the H-bonding and π -stacking directions were aligned with the y- and z-axes, respectively.

The unit cell was then replicated in the x-, y- and z-directions to create larger models $(4\times4\times4)$. Periodic boundary conditions were applied in all three directions to mimic ideal crystalline polymers with infinite chain length and without defects or chain ends. Although the models in this study are approximations of realistic crystalline polymers that have finite length chains with defects and chain ends, the simulation methods developed here can be easily extended in future work to more realistic model structures.

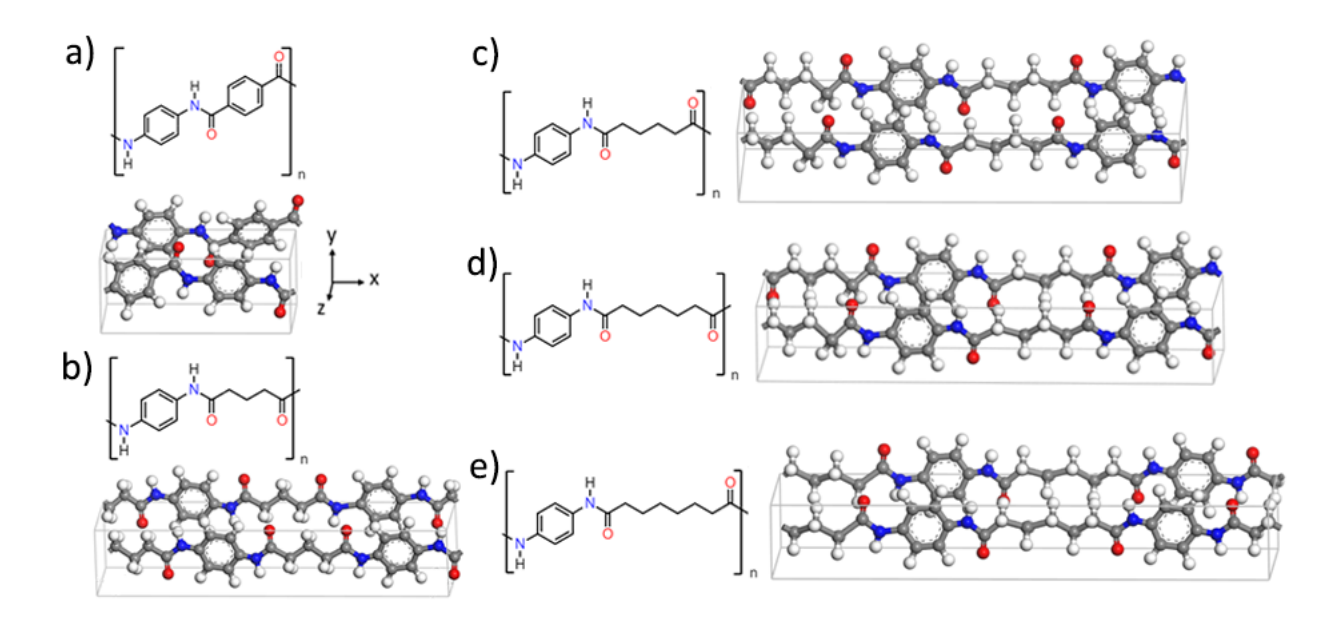


Figure 1: Unit cells of (a) PPTA, (b) PAP5, (c) PAP6, (d) PAP7, and (e) PAP8. The orthogonal directions (x, y, and z) are defined with respect to the perspective views of the unit cells. Atom colors correspond to: oxygen, red; nitrogen, blue; carbon, gray; and hydrogen, white.

In our previous study,⁴⁴ two non-reactive force fields (OPLS (Optimized Potentials for Liquid Simulations)⁴⁶ and CVFF (Consistent Valence Force Field)⁴⁷) and seven different ReaxFF parameterizations were tested for PPTA and PAP5. The results indicated that the ReaxFF force field developed by Liu⁴⁸ was best for studying structure-property relationships of PPTA and PAP5. Since the structure of PAP6, PAP7, and PAP8 are similar to PPTA and PAP5, we used the ReaxFF Liu force field for the simulations here.

All of the MD simulations were carried out using the open-source MD simulation package LAMMPS (Large-scale Atomic/Molecular Massively Parallel Simulator). ⁴⁹ Software OVITO (Open Visualization Tool) ⁵⁰ was used for model visualization. The MD time step was 0.25 fs for all simulations. Temperature and pressure were controlled using a Nosé-Hoover thermostat ⁵¹ and barostat ⁵² with damping parameters of 25 fs and 250 fs, respectively. Each polymer crystal was equilibrated by running simulations in the NPT (constant number of atoms, pressure and temperature) ensemble for 125 ps (until the lattice parameters reached steady-state) at 300 K and 1 atm.

After equilibration, the system was stretched in the chain direction (x-direction) with a strain rate of 1×10^9 s⁻¹ until the total strain reached 25%. The details of the methods were reported in our previous paper. ⁴⁴ The low-strain elastic modulus was calculated by applying a linear fit to the stress-strain data from 0-2% strain, and the high-strain modulus was calculated from the last 5% before failure. The ultimate stress was the stress at the failure strain. These simulations were repeated three times independently with different random velocity seeds before NPT simulation.

Results and Discussion

The stress-strain curves for the polyamides are shown in Fig. 2. The results show that as strain increases, the slope of the curves increases, which indicates the stiffness of the polymers increases with strain. In Fig. 2b, the low-strain and high-strain moduli are plotted as functions of the number of non-aromatic carbons in the polymers. We observe that the high-strain modulus is essentially independent of the number of non-aromatic carbon atoms. This results is supported by the fact that at high strain the modulus is mediated by stretching covalent bonds within the polymer, and these bonds have the about the same strength in all five polymers.

In contrast, the low-strain modulus decreases with increasing number of non-aromatic carbon atoms (Fig. 2b). In our previous study of PPTA and PAP5, ⁴⁴ we found that low strain behavior could be correlated to chain waviness because wavy chains can accommodate strain without stretching covalent bonds. Waviness can be quantified from the distribution of the atoms in the polymer in the plane transverse to the chain direction, i.e., the y-z plane. Fig. 3a is a representative plot of the positions of the non-aromatic carbon atoms and nitrogen atoms in PAP7 with respect to the centroid of each chain, from zero to failure strain. At low strain (darker blue), the atoms are far from the centroid, indicating a wavy structure. Then, as strain increases (lighter blue), the chain is extended, and the atoms are

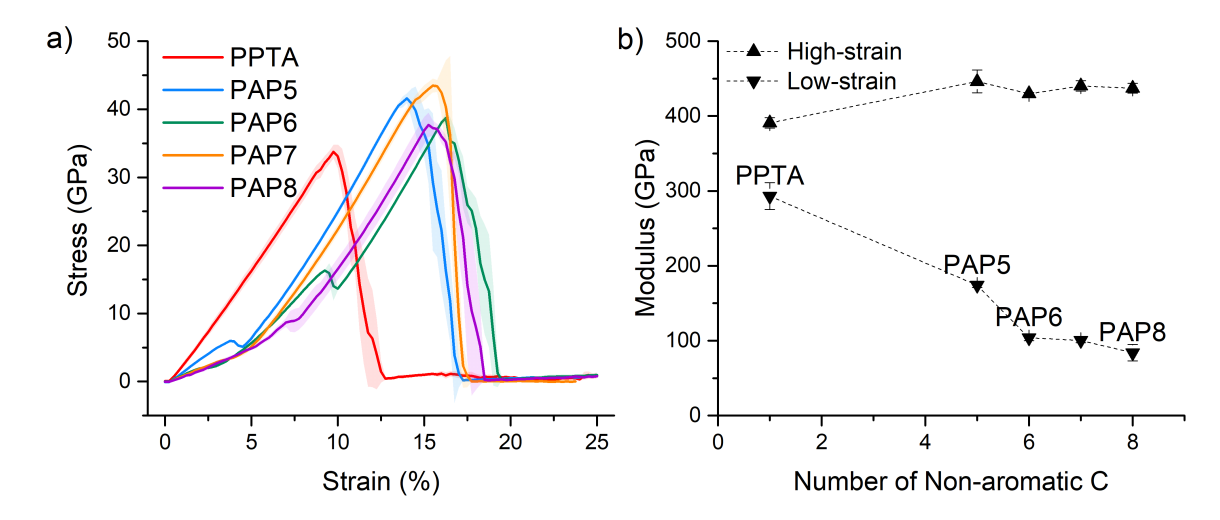


Figure 2: (a) Stress-strain curves for 4x4x4 polyamide crystals strained from 0 to 25% strain. The shaded areas reflect standard deviations calculated from three independent simulations. (b) Low-strain and high-strain modulus as functions of the number of non-aromatic carbons in the diacid monomer of each polymer. Low-strain modulus is calculated from the slope of stress-strain curve from 0 to 2% strain. High-strain modulus is calculated from the last 5% strain before failure.

found closer to the centroid.

Waviness was then calculated as the radius R of a circle fit to the perimeter of 90% of the atoms closest to the center of the chain such that a larger radius corresponds to atoms further from the centroid and wavier chain. The results for all polymers are shown in Fig. 3b, where waviness increases with number of non-aromatic carbons. The increasing trend of waviness is due to the methylene groups acting as spacers between the hydrogen-bonded amide groups, which increases the conformational freedom of the polymer chains. The low-strain modulus is re-plotted in Fig. 3b to show that the decrease in modulus corresponds with increasing waviness.

In Fig. 2, except for PPTA, all of the polymers exhibit a transition (inflection) between low and high strain in the stress-strain curve. Also, for some polymers, there is a sharp shoulder in the stress-strain curve. However, the shapes and sharpness of these transition points are different for the different polymers.

To explore the origin of this behavior, stress-strain simulations were performed for sin-

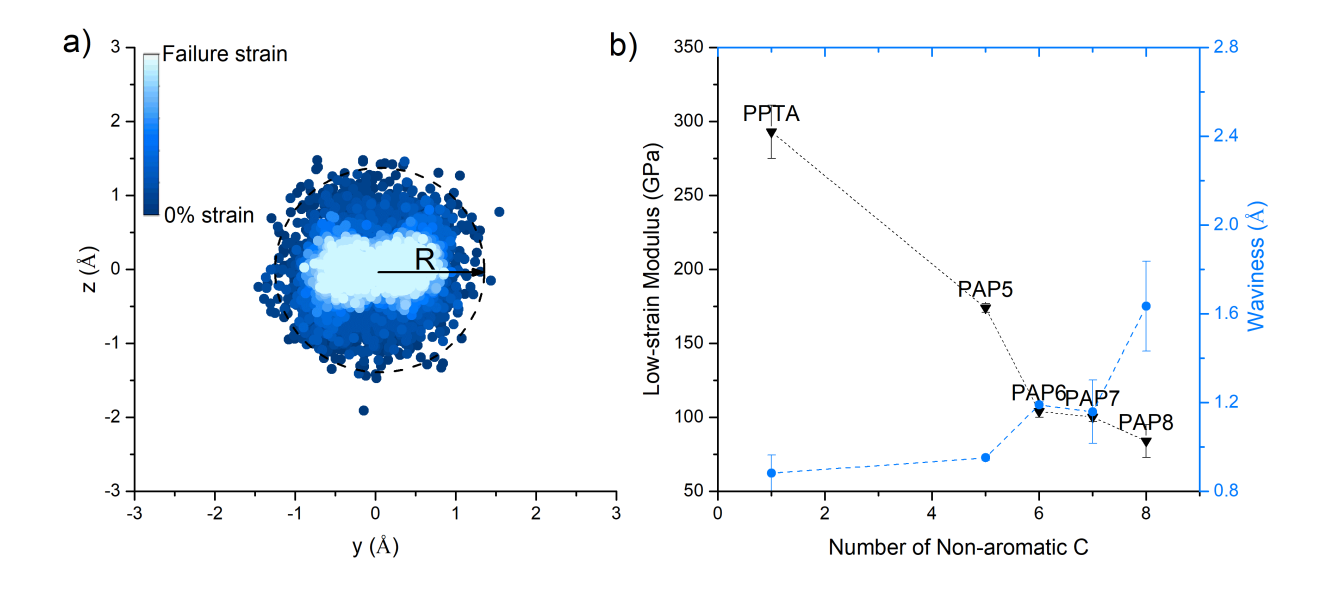


Figure 3: (a) Positions of atoms in the chains projected on the yz plane for PAP7 at zero strain, where the centroid of each chain is manually moved to the origin of the yz plane. Similar plots for the other polymers are shown in Figure S1. The radius R of a circle fit to the outline of 90% of the inner-most non-aromatic carbon atoms and nitrogen atoms averaged over three independent simulations is calculated as a measure of waviness. (b) Low-strain modulus and waviness as functions of the number of non-aromatic carbons. The error bars reflect the standard deviations calculated from three independent simulations.

gle chains taken from the end of the NPT simulation of each crystal. Two representative comparisons between crystals and single chains are shown in Fig. 4. Both single chains and crystals exhibit lower stiffness at low strain than high strain and a gradual increase in stiffness around 5% strain, indicating that this behavior is due to *intra-chain* processes. For PAP6 only (Fig. 4a), the crystal has a sharp transition from low to high strain behavior observed around 10% strain (also observed for PAP8, in Figure S2) while the single chain does not. This indicates that the sharp transition or shoulder in the stress-strain response of some polymers is due to *inter-chain* effects.

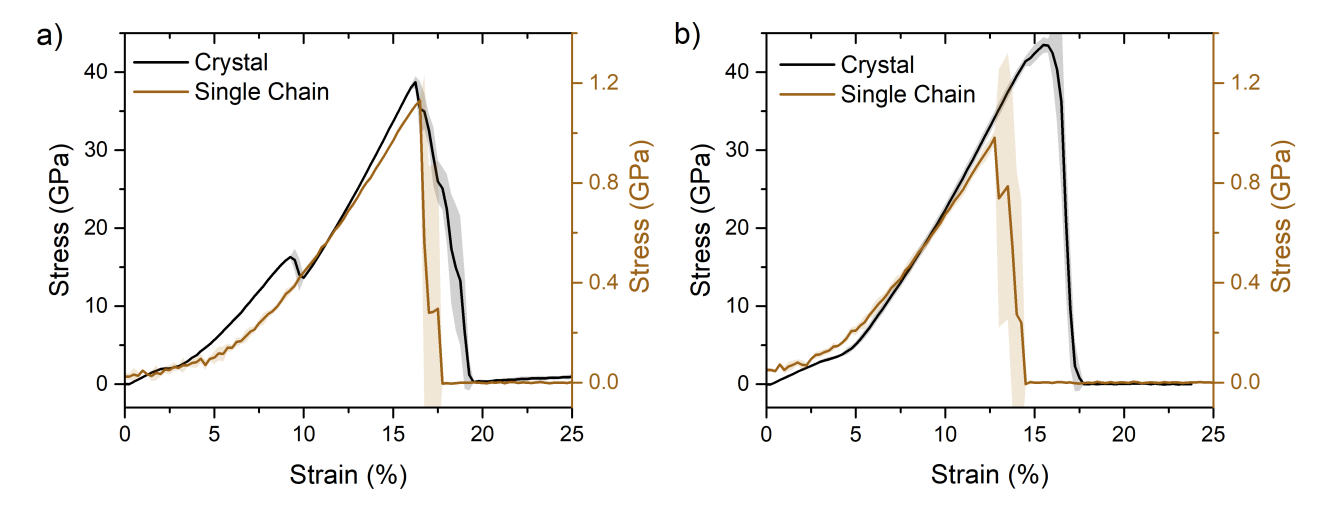


Figure 4: Stress-strain response of single chain and crystal forms of (a) PAP6 and (b) PAP7. The single chain is taken from the end of the NPT simulation of each crystal. Similar trends for PAP5 and PAP8 are shown in Figure S2.

To understand how inter- and intra-chain interactions affect the stress-strain response of the crystals, the movement of the atoms and aromatic rings was characterized in terms of inter-chain slip and rotation of dihedral angles. Inter-chain slip was quantified by the change of average distance in the strain direction between each pair of adjacent aromatic rings in each of the two adjacent chains. Intra-chain dihedral rotation was quantified as the average angles of three different dihedral angles (HNCO, NCCC, and OCCC) inside each chain. The results are plotted vs. strain in Fig. 5.

The motions are quantified by the change of dihedral angles during stretching relative to the equilibrated state at zero strain. The gradual increase in stiffness exhibited by all polymers, except PPTA, correlates well with changes in the dihedral angles (e.g., decreasing OCCC and increasing NCCC at the shoulder), indicating the low strain is accommodated by elongation and rotation of wavy chains. For PAP5-PAP8, the NCCC dihedral angle increases and the OCCC angle decreases gradually at low strain as the stress activates angle rotation.²³ Then, when the chain is fully extended, the angles increase/decrease abruptly and remain at a constant value until failure.

The predominant inter-chain mechanism observed in the simulations is slip between

chains. Slip is near zero for all polymers at low strain. For PPTA, PAP5, and PAP7, the slip remains at zero until failure. However, for PAP6 and PAP8 (animations in Movie S1), there is a sharp increase in slip at the transition between low and high-strain behavior, i.e., the transition between the wavy and extended conformation. This slip mechanism is accessible to PAP6 and PAP8 because they have an even number of carbon atoms, which corresponds to a parallelogram structure that is less stable than the trapezoid structure of polymers with an odd number of carbon atoms $^{53-55}$ (see Figure S3 for representative snapshots of these structures). This so-called odd-even effect 53,56 has been observed in the elastic properties of polymers including α,ω -alkanedicarboxylic acids 57 and polyesters. 58

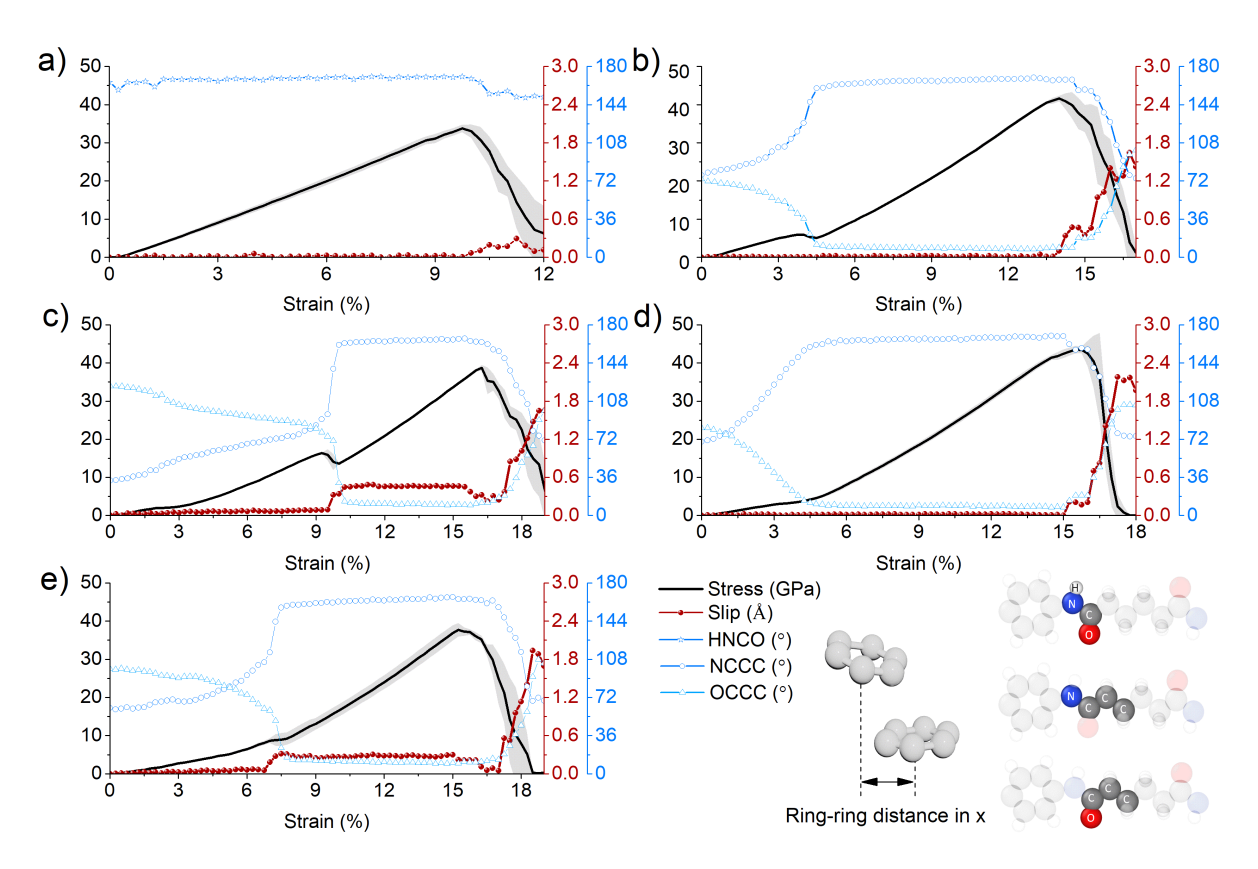


Figure 5: Stress, inter-chain slip, and dihedral angles as functions of strain of (a) PPTA, (b) PAP5, (c) PAP6, (d) PAP7, and (e) PAP8.

Odd-even effects have also been observed in the ultimate properties of polyurethane elastomers ⁵⁹ and polyesters. ⁵⁸ As shown in Fig. 6, aromatic-aliphatic polyamides with an even

number of carbon atoms have lower ultimate stress. Density functional theory calculations (Figure S4) showed that the methylene segment does not directly affect bond strength, suggesting the observed odd-even trend in ultimate stress is an inter-chain effect. First, the slip exhibited by PAP6 and PAP8 (Fig. 5) likely contributes to their lower ultimate strength.

Second, it has been shown that ring-ring interactions (π -stacking) affect the ultimate properties of polyamides, and the strength of these interactions is related to the coplanarity of the rings. ^{44,60} The coplanarity of the rings is quantified by the angle between each pair of aromatic rings in adjacent chains (see inset to Fig. 6) averaged over the last 2% strain before failure. Coplanarity is plotted as a function of the number of non-aromatic carbons in Fig. 6, where small ring-ring angle corresponds to high coplanarity. The ultimate stress and coplanarity of the polymers exhibit consistent trends where polymers with an even number of carbon atoms have less aligned rings and lower strength.

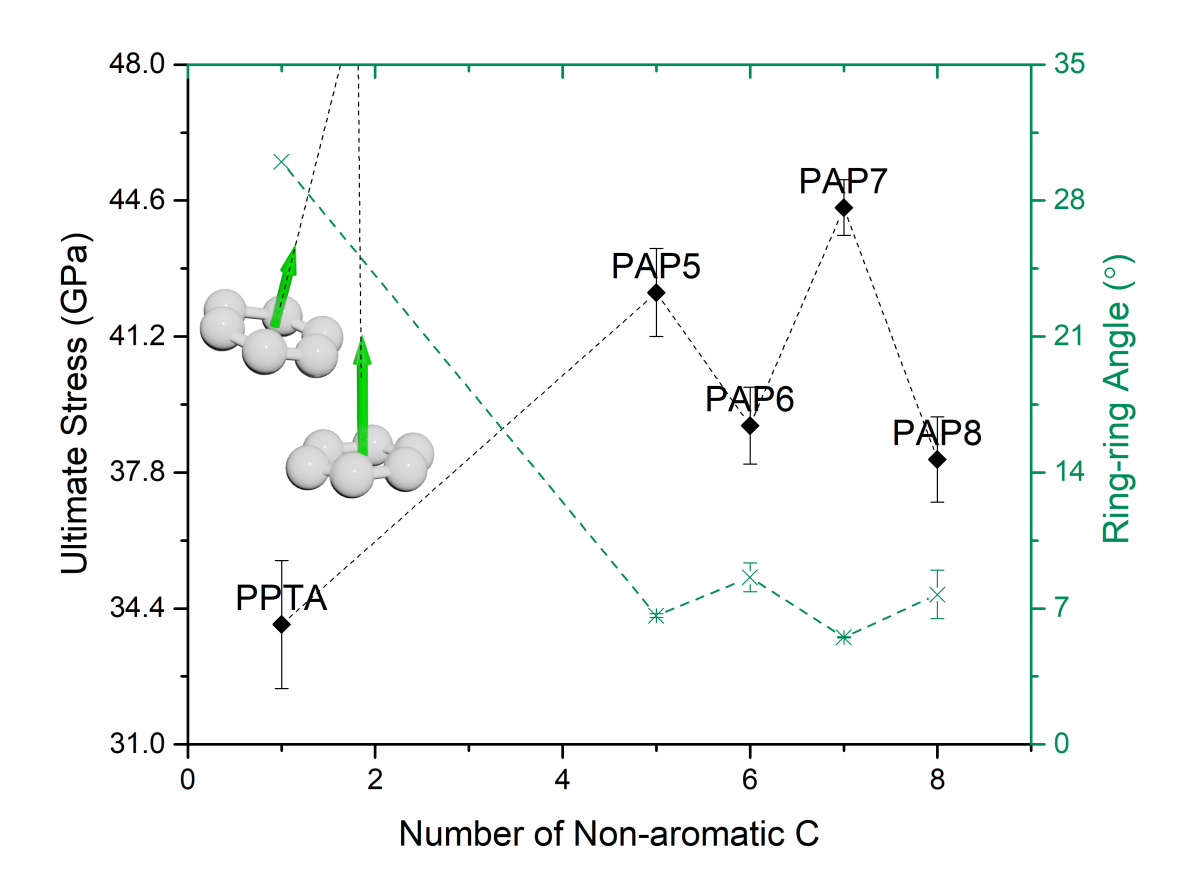


Figure 6: Ultimate stress and coplanarity as functions of the number of non-aromatic carbons. The errors bars reflect the standard deviation from three independent simulations.

Conclusions

Molecular dynamics simulations were performed to study the stress-strain response of PPTA and four related aromatic-aliphatic polyamides (PAP5-PAP8) with different numbers of non-aromatic carbons in the aliphatic chain. It was found that the subtle structural differences between these polymers lead to distinct elastic and ultimate properties. The low-strain modulus (calculated from 0-2% strain) decreased with increasing aliphatic chain length while the high-strain modulus (calculated from the last 5% strain before failure) was independent of the aliphatic chain length. The trend of low-strain modulus was explained in terms of the waviness of the polymers at zero strain, i.e., longer aliphatic chain length increased the

conformational freedom of the chains and therefore increased the waviness of the polymers, which finally decreased the low-strain modulus. The transition from low to high strain behavior was correlated to rotation of dihedral angles as the chains were extended, so this behavior was due to intra-chain effects. It was also observed that polymers with an even number of carbon atoms exhibited inter-chain slip at the transition between the wavy and extended conformation, which was explained by the instability of the trapezoidal structure of these polymers. A similar odd-even effect was observed at failure, where even polymers had lower ultimate stress. Coplanarity of the aromatic rings correlated well with the trend of ultimate stress, i.e., less coplanar rings (larger ring-ring angle) corresponded to lower ultimate stress. The results reported here show that aromatic-aliphatic polyamides can be designed with mechanical properties comparable to or better than PPTA yet even subtle differences in chemical composition can affect properties. Further, the correlations between structure and mechanical properties identified, as well as the simulation-based approach, may be extended to other similar polymers to enable tuning of mechanical properties through chemical modification.

Acknowledgement

We acknowledge ExxonMobil Research and Engineering Company for financial support of this work. The stimulating discussions with ExxonMobil colleagues (Ozcan Altintas, Arben Jusufi, Aruna Mohan, Agostino Pietrangelo, Thomas Sun, Pamela J Wright) are highly appreciated. The simulations were in part run using the Extreme Science and Engineering Discovery Environment (XSEDE), which is supported by National Science Foundation Grant ACI-1548562.

Supporting Information

Movie M1: Animation of strain simulations of all polymers shown from the y-direction (H-bond direction) where all atoms except the aromatic rings are faded to highlight the inter-chain slip.

Movie M2: Animation of strain simulations of all polymers shown x-direction where all atoms except the aromatic rings are faded to highlight the inter-chain slip.

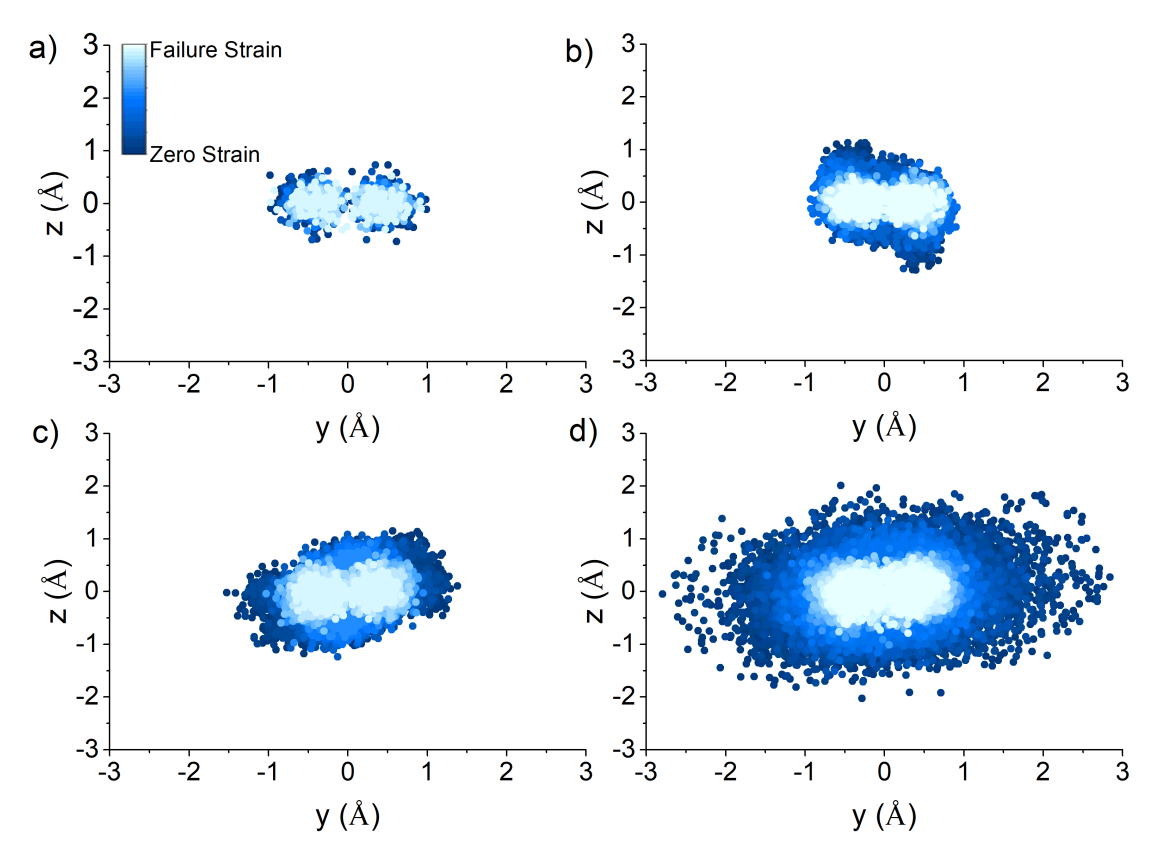


Figure S1: Positions of atoms in the chains projected on the yz plane, where the centroid of each chain is moved to the origin of the yz plane, for (a) PPTA, (b) PAP5, (c) PAP6, and (d) PAP8. The radius of a circle fit to the outline of the 90% innermost non-aromatic carbon atoms is averaged over three independent simulations to quantify waviness.

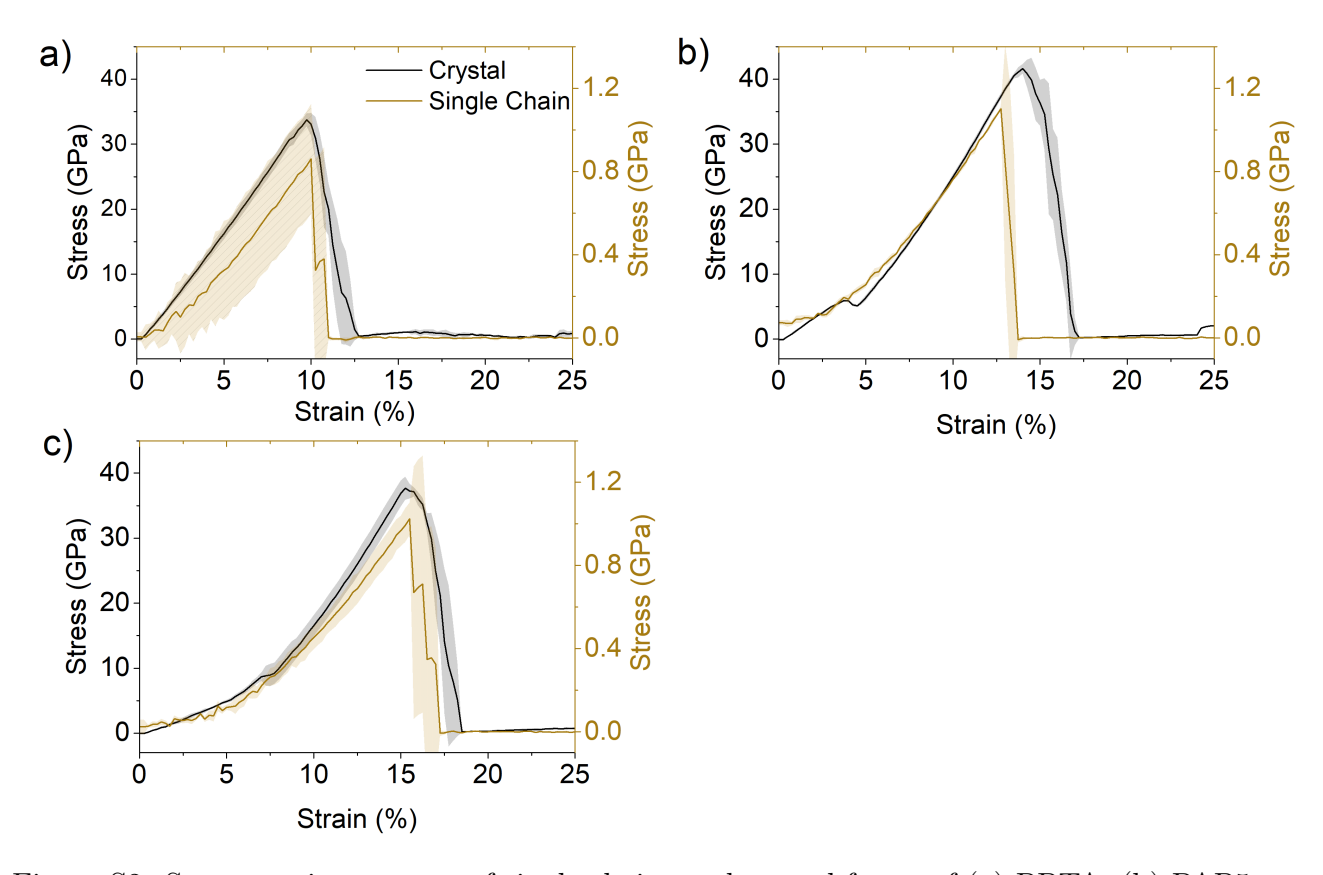


Figure S2: Stress-strain response of single chains and crystal forms of (a) PPTA, (b) PAP5, and (c) PAP8. The single chain is taken from the end of the NPT simulation for each crystal.

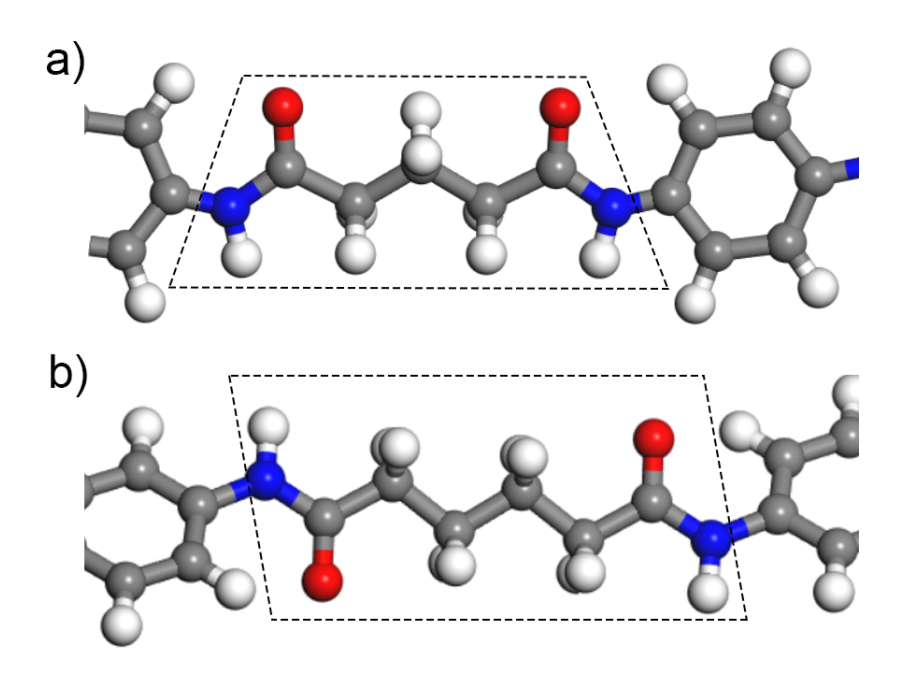


Figure S3: Representative snapshots of trapezoidal and parallelogrammatic structures in the backbones of (a) odd (PAP5) and (b) even (PAP6) polymers.

DFT-computed bond dissociation energy for PPTA and PAP5

Figure S4: Truncated polymer models used to compute the bond dissociation energy (BDE) for (a) PPTA and (b) PAP5. X denotes the bond for which the BDE was computed. For PAP5, the gray part of the repeat unit was omitted from the DFT calculations because the cleaved bond is not likely to be affected by more distant moieties.

Figure S4 shows the model systems used to compute the lowest BDE of the polymer chains for PPTA and PAP5. The bond denoted X was selected based on previous work that showed this bond was the weakest in the PPTA system.⁶¹ To determine the BDE, the bond X was homolytically cleaved leaving two fragments each containing an unpaired electron (doublets). The BDE is then computed from the difference in Gibbs Free Energy between the whole molecule and the sum of the fragments. These calculations were performed in Gaussian 09^{62} at the M062X/6-311+G(2d,p) level of theory.^{63,64}

The computed BDE of bond X was 55.7 kcal/mol for PPTA and 56.3 kcal/mol for PAP5. The 0.6 kcal/mol difference between these two results is within the expected error of this method, which indicates their BDE is nearly equivalent. This calculation was not repeated for PAP6, PAP7, and PAP8 because the longer aliphatic linker in these polymers is not likely to affect the BDE of bond X.

References

- (1) Shim, V.; Lim, C.; Foo, K. Dynamic mechanical properties of fabric armour. *International Journal of Impact Engineering* **2001**, *25*, 1–15.
- (2) Knijnenberg, A.; Bos, J.; Dingemans, T. J. The synthesis and characterisation of reactive poly (p-phenylene terephthalamide) s: a route towards compression stable aramid fibres. *Polymer* 2010, 51, 1887–1897.
- (3) Yang, H. Kevlar aramid fiber; Wiley, 1993.
- (4) Mark, H.; Atlas, S.; Ogata, N. Aromatic polyamide. Journal of Polymer Science 1962, 61, S49–S53.
- (5) Sockalingam, S.; Chowdhury, S. C.; Gillespie Jr, J. W.; Keefe, M. Recent advances in modeling and experiments of Kevlar ballistic fibrils, fibers, yarns and flexible woven textile fabrics—a review. *Textile Research Journal* 2017, 87, 984–1010.
- (6) Kim, J.; McDonough, W. G.; Blair, W.; Holmes, G. A. The modified-single fiber test: A methodology for monitoring ballistic performance. *Journal of applied polymer science* 2008, 108, 876–886.
- (7) Krishnan, K.; Sockalingam, S.; Bansal, S.; Rajan, S. Numerical simulation of ceramic composite armor subjected to ballistic impact. Composites Part B: Engineering 2010, 41, 583–593.
- (8) Rao, Y.; Waddon, A.; Farris, R. Structure–property relation in poly (p-phenylene terephthalamide)(PPTA) fibers. *Polymer* **2001**, *42*, 5937–5946.
- (9) Hogg, P. J. Composites in armor. *Science* **2006**, *314*, 1100–1101.

- (10) Brauckmann, J. O.; Zolfaghari, P.; Verhoef, R.; Klop, E. A.; de Wijs, G. A.; Kentgens, A. P. Structural studies of polyaramid fibers: Solid-state NMR and first-principles modeling. *Macromolecules* **2016**, *49*, 5548–5560.
- (11) Deshmukh, Y. S.; Wilsens, C. H.; Verhoef, R.; Hansen, M. R.; Dudenko, D.; Graf, R.; Klop, E. A.; Rastogi, S. Conformational and structural changes with increasing methylene segment length in aromatic–aliphatic polyamides. *Macromolecules* 2016, 49, 950–962.
- (12) Chen, X. Advanced fibrous composite materials for ballistic protection; Woodhead Publishing, 2016.
- (13) Dobb, M.; Johnson, D.; Majeed, A.; Saville, B. Microvoids in aramid-type fibrous polymers. *Polymer* **1979**, *20*, 1284–1288.
- (14) Debeaupte, E.; Watanabe, M.; Sanui, K.; Ogata, N. In situ polycondensation for synthesis of composites of elastomeric matrixes and wholly aromatic polyamides. *Chemistry of materials* **1992**, *4*, 1123–1128.
- (15) Ferreiro, J. J.; de La Campa, J. G.; Lozano, A. E.; de Abajo, J. Polyisophthalamides with heteroaromatic pendent rings: synthesis, physical properties, and water uptake. Journal of Polymer Science Part A: Polymer Chemistry 2005, 43, 5300–5311.
- (16) Ferrero, E.; Espeso, J.; De la Campa, J.; De Abajo, J.; Lozano, A. Synthesis and characterization of aromatic polyamides containing alkylphthalimido pendent groups.

 *Journal of Polymer Science Part A: Polymer Chemistry 2002, 40, 3711–3724.
- (17) Zhou, S.; Zhang, M.; Wang, R.; Ping, J.; Zhang, X.; Zhao, N.; Xu, J.; Shen, Z.; Fan, X. Synthesis and characterization of new aramids based on o-(m-triphenyl)-terephthaloyl chloride and m-(m-triphenyl)-isophthaloyl chloride. *Polymer* **2017**, *109*, 49–57.

- (18) García, J. M.; García, F. C.; Serna, F.; José, L. High-performance aromatic polyamides. Progress in polymer science **2010**, 35, 623–686.
- (19) Huang, Y.-C.; Wang, K.-L.; Chang, C.-H.; Liao, Y.-A.; Liaw, D.-J.; Lee, K.-R.; Lai, J.-Y. Solvent Response and Protonation Effects of Novel Aramides Containing Pyridine and Unsymmetrical Carbazole Moieties. *Macromolecules* 2013, 46, 7443–7450.
- (20) Rutledge, G.; Suter, U.; Papaspyrides, C. Analysis of structure of polymorphism in poly (p-phenyleneterephthalamide) through correlation of simulation and experiment. *Macromolecules* 1991, 24, 1934–1943.
- (21) Crouch, I.; Arnold, L.; Pierlot, A.; Billon, H. *The science of armour materials*; Elsevier, 2017; pp 269–330.
- (22) Brown, J.; Ennis, B. Thermal analysis of Nomex® and Kevlar® fibers. Textile Research Journal 1977, 47, 62–66.
- (23) Tonelli, A. E.; Edwards, J. F. Are poly (p-phenylene terephthalamide) (Kevlar®) and other liquid crystalline polymers conformationally rigid? *Polymer* **2020**, *193*, 122342.
- (24) Khademinejad, S.; Mehdipour-Ataei, S.; Ziaee, F.; Abbasi, F. Poly (ether ether sulfone amide) s as a new category of processable heat-resistant polymers. *Designed Monomers and Polymers* **2016**, *19*, 553–559.
- (25) Liou, G.-S.; Fang, Y.-K.; Yen, H.-J. Synthesis and properties of noncoplanar rigid-rod aromatic polyamides containing phenyl or naphthyl substituents. *Journal of Polymer Research* **2007**, *14*, 147–155.
- (26) Amininasab, S. M.; Rashidi, A.; Taghavi, M.; Shami, Z. Preparation and characterization of novel thermostable polyamides bearing different photoactive pendent architectures with antibacterial properties. Chinese Journal of Polymer Science 2016, 34, 766–776.

- (27) Hajibeygi, M.; Shabanian, M.; Khodaei-Tehrani, M. New heat resistant nanocomposites reinforced silicate nanolayers containing triazine rings based on polyamide: synthesis, characterization, and flame retardancy study. *Polymer Composites* **2016**, *37*, 188–198.
- (28) Zou, F.; Wen, H.; Yan, T.; Cai, M. Synthesis and properties of novel soluble aromatic polyamides containing 4-aryl-2, 6-diphenylpyridine moieties and pendant fluorinated phenoxy groups. *Journal of Polymer Research* **2016**, *23*, 1–10.
- (29) Zhang, G.; Yan, G.-M.; Ren, H.-H.; Li, Y.; Wang, X.-J.; Yang, J. Effects of a transor cis-cyclohexane unit on the thermal and rheological properties of semi-aromatic polyamides. *Polymer Chemistry* **2016**, *7*, 44–53.
- (30) Damaceanu, M.-D.; Rusu, R.-D.; Nicolescu, A.; Bruma, M.; Rusanov, A. L. Organosoluble asymmetric aromatic polyamides bearing pendent phenoxy groups. *Polymer in*ternational **2011**, 60, 1248–1258.
- (31) Long, J.-W.; Chen, L.; Liu, B.-W.; Shi, X.-H.; Lin, X.-B.; Li, Y.-M.; Wang, Y.-Z. Tuning the Pendent Groups of Semiaromatic Polyamides toward High Performance.

 *Macromolecules** 2020, 53, 3504–3513.
- (32) Peng, S.; Peng, L.; Yi, C.; Zhang, W.; Wang, X. A novel synthetic strategy for preparing semi-aromatic components modified polyamide 6 polymer. *Journal of Polymer Science Part A: Polymer Chemistry* **2018**, *56*, 959–967.
- (33) Bakkali-Hassani, C.; Planes, M.; Roos, K.; Wirotius, A.-L.; Ibarboure, E.; Carlotti, S. Synthesis of polyamide 6 with aramid units by combination of anionic ring-opening and condensation reactions. *European Polymer Journal* **2018**, *102*, 231–237.
- (34) Rwei, S.-P.; Ranganathan, P.; Chiang, W.-Y.; Lee, Y.-H. Synthesis and characterization of copolyamides derived from novel aliphatic bio-based diamine. *Journal of Applied Polymer Science* **2018**, *135*, 46878.

- (35) Rwei, S.-P.; Ranganathan, P.; Chiang, W.-Y.; Lee, Y.-H. Synthesis of low melting temperature aliphatic-aromatic copolyamides derived from novel bio-based semi aromatic monomer. *Polymers* **2018**, *10*, 793.
- (36) Bisoi, S.; Mandal, A. K.; Padmanabhan, V.; Banerjee, S. Aromatic polyamides containing trityl substituted triphenylamine: Gas transport properties and molecular dynamics simulations. *Journal of Membrane Science* **2017**, *522*, 77–90.
- (37) Prevorsek, D. C.; Kwon, Y. D.; Chin, H. B. Analysis of the temperature rise in the projectile and extended chain polyethylene fiber composite armor during ballistic impact and penetration. *Polymer Engineering & Science* **1994**, *34*, 141–152.
- (38) Cline, J.; Wu, V.; Moy, P. Assessment of the Tensile properties for single fibers; 2018.
- (39) Tashiro, K.; Kobayashi, M.; Tadokoro, H. Elastic moduli and molecular structures of several crystalline polymers, including aromatic polyamides. *Macromolecules* 1977, 10, 413–420.
- (40) Moe, N. E.; Ediger, M. Molecular dynamics computer simulation of polyisoprene local dynamics in dilute toluene solution. *Macromolecules* **1995**, *28*, 2329–2338.
- (41) Zhang, B.; Liu, R.; Zhang, J.; Liu, B.; He, J. MesoDyn simulation study of phase behavior for dye-polyether derivatives in aqueous solutions. *Computational and Theoretical Chemistry* **2016**, *1091*, 8–17.
- (42) Zhelavskyi, O. S.; Kyrychenko, A. Atomistic molecular dynamics simulations of the LCST conformational transition in poly (N-vinylcaprolactam) in water. *Journal of Molecular Graphics and Modelling* **2019**, *90*, 51–58.
- (43) Chantawansri, T. L.; Yeh, I.-C.; Hsieh, A. J. Investigating the glass transition temperature at the atom-level in select model polyamides: A molecular dynamics study. *Polymer* **2015**, *81*, 50–61.

- (44) Yang, Q.; Li, W.; Stober, S. T.; Burns, A. B.; Gopinadhan, M.; Martini, A. Molecular Dynamics Simulation of the Stress–Strain Behavior of Polyamide Crystals. *Macro-molecules* **2021**, *54*, 8289–8302.
- (45) BIOVIA, BIOVIA Material Studio. 2020; http://www.3ds.com/products-services/biovia/products/molecular-modeling-simulation/biovia-materials-studio,

 Last accessed 16 February 2021.
- (46) Dodda, L. S.; Cabeza de Vaca, I.; Tirado-Rives, J.; Jorgensen, W. L. LigParGen web server: an automatic OPLS-AA parameter generator for organic ligands. *Nucleic acids research* **2017**, *45*, W331–W336.
- (47) Dauber-Osguthorpe, P.; Roberts, V. A.; Osguthorpe, D. J.; Wolff, J.; Genest, M.; Hagler, A. T. Structure and energetics of ligand binding to proteins: Escherichia coli dihydrofolate reductase-trimethoprim, a drug-receptor system. *Proteins: Structure, Function, and Bioinformatics* 1988, 4, 31–47.
- (48) Liu, L.; Liu, Y.; Zybin, S. V.; Sun, H.; Goddard III, W. A. ReaxFF-lg: Correction of the ReaxFF reactive force field for London dispersion, with applications to the equations of state for energetic materials. *The Journal of Physical Chemistry A* 2011, 115, 11016– 11022.
- (49) Plimpton, S. Fast parallel algorithms for short-range molecular dynamics. *Journal of computational physics* **1995**, *117*, 1–19.
- (50) Stukowski, A. Visualization and analysis of atomistic simulation data with OVITO-the Open Visualization Tool. *Modelling and Simulation in Materials Science and Engineering* **2009**, *18*, 015012.
- (51) Hoover, W. G. Canonical dynamics: Equilibrium phase-space distributions. *Physical review A* **1985**, *31*, 1695.

- (52) Hoover, W. G. Constant-pressure equations of motion. *Physical Review A* **1986**, *34*, 2499.
- (53) Thalladi, V. R.; Nüsse, M.; Boese, R. The melting point alternation in α, ω-alkanedicarboxylic acids. Journal of the American Chemical Society 2000, 122, 9227–9236.
- (54) White, N. A.; Ellis, H. A. Room temperature structures and odd–even behaviour of a homologous series of anhydrous lithium n-alkanoates. *Journal of Molecular Structure* 2008, 888, 386–393.
- (55) Bond, A. D. On the crystal structures and melting point alternation of the n-alkyl carboxylic acids. *New journal of chemistry* **2004**, *28*, 104–114.
- (56) Baeyer, A. Ueber regelmässigkeiten im schmelzpunkt homologer verbindungen. Berichte der deutschen chemischen Gesellschaft 1877, 10, 1286–1288.
- (57) Mishra, M. K.; Varughese, S.; Ramamurty, U.; Desiraju, G. R. Odd–even effect in the elastic modulii of α , ω -alkanedicarboxylic acids. *Journal of the American Chemical Society* **2013**, 135, 8121–8124.
- (58) Shen, Y.; Yao, B.; Yu, G.; Fu, Y.; Liu, F.; Li, Z. Facile preparation of bio-based polyesters from furandicarboxylic acid and long chain diols via asymmetric monomer strategy. *Green Chemistry* **2017**, *19*, 4930–4938.
- (59) Prisacariu, C.; Scortanu, E. Influence of the type of chain extender and urethane group content on the mechanical properties of polyurethane elastomers with flexible hard segments. *High Performance Polymers* **2011**, *23*, 308–313.
- (60) Burattini, S.; Greenland, B. W.; Hayes, W.; Mackay, M. E.; Rowan, S. J.; Colquhoun, H. M. A supramolecular polymer based on tweezer-type π π stacking

- interactions: molecular design for healability and enhanced toughness. *Chemistry of Materials* **2011**, *23*, 6–8.
- (61) Mercer, B.; Zywicz, E.; Papadopoulos, P. Molecular dynamics modeling of PPTA crystallite mechanical properties in the presence of defects. *Polymer* **2017**, *114*, 329–347.
- (62) Frisch, M. J. et al. Gaussian o9 Revision E.01. 2013; Gaussian Inc. Wallingford CT.
- (63) Zhao, Y.; Truhlar, D. G. The M06 suite of density functionals for main group ther-mochemistry, thermochemical kinetics, noncovalent interactions, excited states, and transition elements: two new functionals and systematic testing of four M06-class functionals and 12 other functionals. Theoretical Chemistry Accounts 2008, 120, 215–241.
- (64) McLean, A. D.; Chandler, G. S. Contracted Gaussian basis sets for molecular calculations. I. Second row atoms, Z=11-18. The Journal of Chemical Physics 1980, 72, 5639-5648.